

A TLK2-mediated calcium-driven cell death pathway links neuronal degeneration to nuclear envelope disruption

Received: 30 July 2024

Accepted: 1 April 2025

Published online: 10 April 2025

 Check for updatesYajie Li^{1,2}, Huaiyuan Huang¹, Jingwen Gao¹, Jinhong Lu¹, Guifeng Kang³,
Yipeng Ge⁴, Wencan Jiang^{5,6}, Xiang Cai², Guojun Zhang^{5,6} ✉ &
Lei Liu^{1,6} ✉

Calcium overload drives neuronal cell death, but its mechanisms remain unclear. Previous studies in *Drosophila* implicated tousel-like kinase (TLK) in this process. Here, we investigated TLK2, the mammalian homolog, in calcium overload-induced neuronal death. We found that calcium overload enhances TLK2 expression, multimerization, and phosphorylation, increasing its kinase activity. Inhibiting TLK2 via RNA interference or a small-molecule inhibitor reduced neuronal death, while TLK2 overexpression triggered nuclear envelope (NE) rupture, nuclear enlargement, multinucleation, and cell cycle reentry markers. A protein complex involving TLK2, dynein light chain LC8, and myosin IIA was linked to NE disruption. In mouse models of glaucoma, TLK2 contributed to retinal ganglion cell degeneration, connecting calcium overload to neurodegeneration. We propose “CaToptosis” (Calcium-induced Tousel-like kinase-mediated cell death) as a distinct neuronal death pathway.

Calcium overload, characterized by disrupted calcium homeostasis and gradual increases in intracellular calcium levels, serves as a biomarker for brain aging and neurodegenerative diseases such as Alzheimer’s disease (AD) and Parkinson’s disease (PD)¹. Notably, calcium overload also occurs in glaucoma. Evidence indicates that tissue hypoxia or ischemia, due to vascular disruption, occurs in both normal-tension and hypertensive glaucoma². In cultured cells, hypoxia can significantly induce calcium overload, suggesting that hypoxia in glaucoma may lead to calcium overload damage^{3,4}.

In contrast to calcium overload, excitotoxicity is mediated by a brief episode of ischemia, which induces neuronal death by excessive glutamate release. In general, calcium toxicity in neurons may trigger diverse cell death pathways, such as apoptosis, mitochondrial permeability transition (MPT)-driven necrosis, necroptosis, and ferroptosis⁵.

Using *Drosophila* genetics, we developed models of calcium overload and excitotoxicity by controlling the expression of the glutamate receptor 1 lurcher mutant (GluRI^{LC}), a constantly open cation channel with calcium permeability about twice that of sodium⁶. In the excitotoxicity model, loss of function of calpain and cathepsin suppressed neuronal necrosis, similar to findings in *C. elegans* and mammalian systems^{7,8}. In contrast, under conditions of calcium overload, we identified a distinct set of modulators. Notably, the loss of tousel-like kinase (TLK) was associated with a significant reduction in cell death, highlighting its potential role in modulating cellular responses to calcium dysregulation⁹. Moreover, TLK-mediated cell death occurs during normal development, and overexpression of TLK directly induces cell death⁹. These studies suggest that the genes regulating calcium overload are likely different from those involved in excitotoxicity, a phenomenon also suggested by others¹⁰.

¹Department of Biochemistry and Molecular Biology School of Basic Medicine, Capital Medical University, Youanmen, Beijing 100069, China. ²Oujiang Laboratory, School of Mental Health, Wenzhou Medical University, Wenzhou, Zhejiang 325035, China. ³School of Pharmaceutical Sciences, Capital Medical University, Youanmen, Beijing 100069, China. ⁴Department of Cardiovascular Surgery, Beijing Anzhen Hospital, Capital Medical University, Anzhen Road 2#, Chaoyang District, Beijing 10029, China. ⁵Department of Clinical Diagnosis, Laboratory of Beijing Tiantan Hospital and Capital Medical University, Beijing 100070, China. ⁶Laboratory diagnosis platform for nervous system infectious diseases, Laboratory for Clinical Medicine, Capital Medical University, Beijing 100070, China. ✉ e-mail: guojun.zhang@ccmu.edu.cn; leiliu@ccmu.edu.cn

In this study, we identified a biomarker for calcium overload in mammalian neurons, distinguishing it from excitotoxicity. We also focused on TLK2, the mammalian homolog of *Drosophila* TLK, and demonstrated its critical role in calcium overload-induced cell death in primary neurons and HEK293 cells. Remarkably, TLK2 acts as a key mediator of cell death, as it is both necessary and sufficient for regulating this process. Moreover, therapeutic targeting of TLK2 significantly suppressed neuronal cell death in mouse models of glaucoma, underscoring its potential as a promising intervention target.

Results

Increased TLK2 levels act as both a biomarker and a regulator of cell death induced by calcium overload

In our previous study, we found that driving expression of *GluRI^{Lc}* using a *heat shock (hs)* promoter at room temperature led to a gradual increase in intracellular calcium ion concentration ($[Ca^{2+}]_i$). After 7 days of *GluRI^{Lc}* activation, significant cell death was observed in the fly eye tissues. Genetic screening revealed that the cell death induced by low-level expression of *GluRI^{Lc}* was primarily mediated by TLK (Tousled-Like Kinase)¹¹. To explore the conservation of TLK2 function in mammalian cells, we employed primary cultured neuronal cells and treated them with ionomycin, a calcium ionophore, to induce calcium overload¹². Treatment with ionomycin at concentrations of 0.5, 1, and 1.5 μ M led to a pronounced increase in TLK2 protein levels. However, at higher ionomycin concentrations, TLK2 levels declined relative to those observed at 1 μ M, suggesting a concentration-dependent regulation of TLK2 expression (Fig. 1A). Measurements of $[Ca^{2+}]_i$ using Fura-2 showed that after 1 hour of treatment, $[Ca^{2+}]_i$ increased from a baseline of 80.90 nM to 264.30 nM (3.3-fold), 319.9 nM (4.0-fold), and 477.58 nM (5.9-fold) at 0.5, 1, and 1.5 μ M ionomycin, respectively, with no cell death. However, after 48 hours, cell death occurred in 35%, 46.2%, and 52% of the cells at these respective concentrations (Fig. 1B, C). At ionomycin concentrations $\geq 3 \mu$ M, $[Ca^{2+}]_i$ rapidly increased to 806.84 nM (10-fold) within 10 minutes, with cell viability maintained for up to 1 hour; however, 74.4% cell death was observed after 48 hours. At 5 μ M ionomycin, $[Ca^{2+}]_i$ spiked to 1363.32 nM (16.9-fold), resulting in 55% cell death within 1 hour and 87% death after 24 hours (Fig. 1B, C). To further investigate the role of TLK2 in this process, we used self-complementary AAV2 to express TLK2 shRNA and effectively knock down TLK2 expression in primary neurons (Fig. 1D). TLK2 knockdown significantly attenuated cell death induced by ionomycin at 0.5, 1, and 1.5 μ M but had no protective effect at 3 or 5 μ M ionomycin (Fig. 1E). As a marker of excitotoxicity, we assessed calpain activation, which cleaves its substrate P35, AIF and SPTAN1¹³. We observed increased P35, AIF and SPTAN1 cleavage in cells treated with 1.5, 3, and 5 μ M ionomycin, coinciding with reduced TLK2 levels (Fig. 1A, F, Supplementary Fig. 1A, B). The levels of TLK2 and P35 cleavage were measured in response to ionomycin treatment (0–10 μ M) and plotted to reveal their relationship (Fig. 1G). These findings indicate that calcium overload is characterized by a 3.3- to 4.0-fold increase in intracellular calcium concentration ($[Ca^{2+}]_i$) and a corresponding upregulation of TLK2. In contrast, excitotoxicity, marked by a more substantial rise in $[Ca^{2+}]_i$ (5.9-fold or higher), is associated with calpain activation but does not involve TLK2 upregulation.

To investigate whether TLK2 upregulation could serve as a general biomarker of calcium overload, we examined MCF7 breast cancer cells, which are known to express high levels of TLK2 to support cancer progression¹⁴. Ionomycin treatment at concentrations of 1–10 μ M induced a transient increase in $[Ca^{2+}]_i$, which rapidly returned to baseline (Supplementary Fig. 1C). Notably, MCF7 cells demonstrated efficient regulation of $[Ca^{2+}]_i$ levels, with ionomycin concentrations within this range stimulating cell growth, whereas higher concentrations resulted in cell death (Supplementary Fig. 1D, E). These findings suggest a distinct response to calcium overload in MCF7 cells

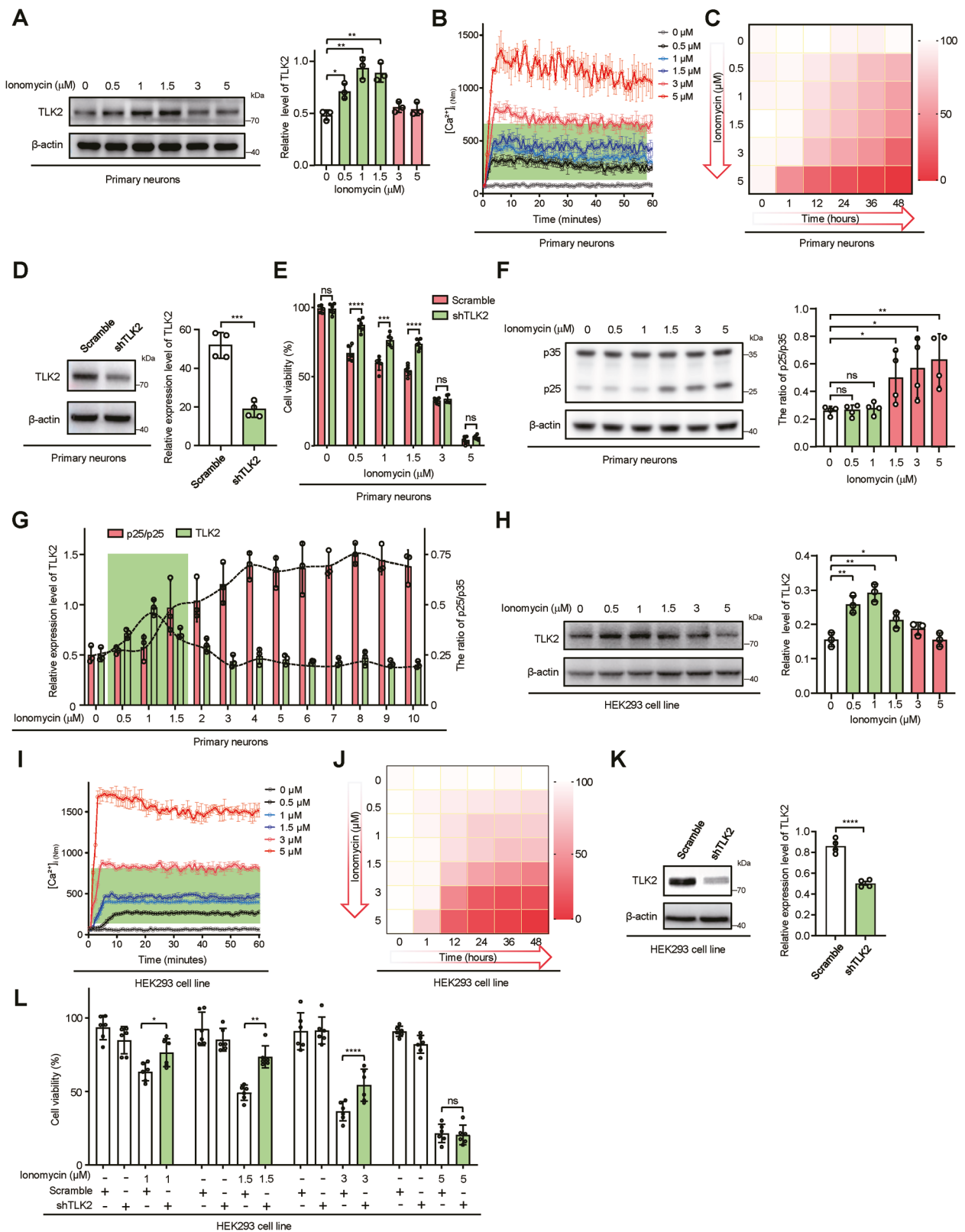
compared to neurons, reflecting differences in calcium handling and cellular outcomes between these cell types.

HEK293 cells, a human embryonic kidney cell line, exhibited a response to ionomycin similar to that of primary neurons, including a dose-dependent increase in $[Ca^{2+}]_i$, changes in TLK2 expression, and subsequent cell death (Fig. 1H–J). TLK2 knockdown in HEK293 cells using TLK2 shRNA resulted in significant resistance to ionomycin-induced cell death at ionomycin concentrations $\leq 3 \mu$ M, but not at 5 μ M (Fig. 1K–L). Promethazine (PMZ) inhibited TLK2 activity in a kinase assay (Supplementary Fig. 1F), similar to its known inhibition of TLK1¹⁵. Cell death induced by calcium overload was rescued by PMZ in HEK293 cells (Supplementary Fig. 1G), suggesting TLK2 kinase maybe involved the cell death process. These results suggest that TLK2 upregulation serves as a biomarker for calcium overload and plays a critical role in regulating calcium overload-induced cell death in both primary neurons and HEK293 cells.

TLK2 overexpression induces a distinct form of cell death characterized by nuclear envelope (NE) rupture

TLK2 is known to undergo hyperphosphorylation and form oligomers, which in turn enhances its kinase activity¹⁶. In HEK293 cells treated with ionomycin, a similar gain-of-function effect was observed, with increased oligomer formation and phosphorylation (Fig. 2A, B). This suggests that both oligomerization and phosphorylation are key factors amplifying TLK2's kinase activity. Since multiple pathways are involved in calcium overload-induced cytotoxicity¹⁷, we developed a model specifically to investigate TLK2-mediated cell death. Given that TLK2 activity is enhanced during calcium overload, we focused on its gain-of-function. We generated a Teton-inducible TLK2-overexpressing HEK293 stable cell line. Upon doxycycline administration, TLK2 expression was significantly increased (Fig. 2C), accompanied by phosphorylation and oligomerization of TLK2 (Fig. 2D, E). Cell death assays revealed that overexpression of TLK2 induces a gradual increase in cell death over 24 and 48 hours following TLK2 induction (Fig. 2F). Under physiological conditions, TLK2 is predominantly localized in the nucleus¹⁶. However, in response to calcium overload, TLK2 accumulates around the NE and overlaps with a marker of the nuclear pore complex (NPC) (Fig. 2G). Notably, the integrity of the NE appears to be compromised, exhibiting a discontinuous pattern, which is indicative of NE damage (Fig. 2G). To confirm these findings, we employed a NE extraction assay to isolate the nuclear membrane. By using lamin B1, a protein of the nuclear lamina, as a reference, we detected an increased presence of TLK2 in the isolated nuclear membrane following ionomycin treatment (Fig. 2H). To assess the extent of NE damage, we expressed a GFP-tagged nuclear protein (Np-GFP) in both wild-type and TLK2 knockout (KO) cells. Upon ionomycin treatment (1 μ M), a rapid leakage of GFP from the nucleus into the cytoplasm was observed in wild-type cells, but not in TLK2 KO cells (Fig. 2I and Supplementary Movie 1). NE integrity loss was also observed in TLK2 overexpression cells (Fig. 2J). This loss of NE integrity, under conditions of calcium overload and TLK2 overexpression, led to an increase in the levels of γ H2AX, a marker of DNA damage¹⁸ (Supplementary Fig. 2A, B).

The TLK2-induced cell death was significantly reduced by PMZ, a known inhibitor of TLK2 kinase activity (Fig. 2F), confirming that cell death is dependent on TLK2 kinase activity. In contrast, other inhibitors—such as MG-101 (calpain inhibitor), Z-VAD-fmk (an apoptosis inhibitor), Necrostatin-1 (a necroptosis inhibitor), and Ferrostatin-1 (a ferroptosis inhibitor)—had no effect on the cell death caused by TLK2 overexpression (Fig. 2F). Moreover, we observed no activation of the apoptosis marker caspase-3 (Supplementary Fig. 2C), and transcription levels of the necroptosis marker MLKL, as well as ferroptosis markers SLC7A11 and GPX4, remained unchanged (Supplementary Fig. 2D–F). To further classify the cell death, we evaluated plasma membrane integrity. Annexin V staining was positive, indicating



phosphatidylserine exposure, which is characteristic of early apoptosis. However, despite cell swelling, propidium iodide (PI) staining was negative (Fig. 2K), suggesting that the morphological features of cell death were more consistent with apoptosis rather than other forms of programmed necrosis¹⁹. These results indicate that TLK2 gain-of-function-induced cell death is distinct from existing pathways of programmed cell death.

Neurons are vulnerable to NE damage than HEK293 cells

To overexpress TLK2 in primary neurons, we created a Cre-mediated conditional expression system by inserting TLK2 cDNA into the Rosa26 locus (Supplementary Fig. 3A). We collected embryonic brains and made primary neuron cultures. Then, scAAV2/9-CMV-Cre was infected, end up with approximately 70% transfection efficiency (Supplementary Fig. 3B). Our results showed that a three-fold increase in TLK2

Fig. 1 | TLK2 knockdown rescues calcium overload-induced cell death.

A Western blot analysis of TLK2 protein levels in primary cultured neurons treated with varying concentrations of ionomycin (0, 0.5, 1, 1.5, 3, 5 μM). A quantitative statistical analysis was performed to determine relative TLK2 protein expression ($n = 3$ independent experiments). **B** Measurement of cytosolic $[\text{Ca}^{2+}]_i$ changes in Fura-2-loaded primary cultured neurons exposed to different ionomycin concentrations (0, 0.5, 1, 1.5, 3, 5 μM) ($n = 3$ independent experiments). The green background represents the range of $[\text{Ca}^{2+}]_i$ that can increase TLK2 protein expression. **C** Cell viability was assessed using CCK-8 assays. A heatmap was generated to compare the relative viability of primary cultured neurons treated with different ionomycin concentrations (0, 0.5, 1, 1.5, 3, 5 μM) across various time points (0, 1, 12, 24, 36, and 48 hours), providing a comprehensive overview of the dose- and time-dependent effects of ionomycin on neuronal viability ($n = 3$ independent experiments). **D** Western blot analysis of TLK2 protein expression in primary cultured neurons infected with scAAV carrying scramble or TLK2 shRNA. Quantitative analysis of relative TLK2 protein levels was conducted ($n = 4$ independent experiments). **E** Cell viability of primary cultured neurons infected with scAAV carrying scramble or TLK2 shRNA under various ionomycin concentrations (0, 1.0, 1.5, 3, 5 μM) was assessed ($n = 6$ independent experiments). **F** Western blot detection of P35 cleavage in primary cultured neurons treated with different concentrations of ionomycin (0, 0.5, 1, 1.5, 3, 5 μM). Quantitative statistical analysis of

the ratio of p25 to p35 was performed ($n = 4$ independent experiments).

G Graphical representation of TLK2 expression levels and the p25/p35 ratio in primary neurons treated with various concentrations of ionomycin ($n = 3$ independent experiments). The green background represents the range of $[\text{Ca}^{2+}]_i$ that can increase TLK2 protein expression. **H** Western blot analysis of TLK2 protein levels in HEK293 cells treated with varying concentrations of ionomycin (0, 0.5, 1, 1.5, 3, 5 μM). Quantitative analysis of relative TLK2 protein levels was performed ($n = 3$ independent experiments). **I** Changes in cytosolic $[\text{Ca}^{2+}]_i$ in Fura-2-loaded HEK293 cells treated with different ionomycin concentrations (0, 0.5, 1, 1.5, 3, 5 μM) were measured ($n = 3$ independent experiments). The green background represents the range of $[\text{Ca}^{2+}]_i$ that can increase TLK2 protein expression. **J** Heatmap comparing relative cell viability in HEK293 cells treated with different ionomycin concentrations (0, 0.5, 1, 1.5, 3, 5 μM) across multiple time points (0, 1, 12, 24, 36, 48 hours) ($n = 3$ independent experiments). **K** Western blot analysis of TLK2 protein expression levels in HEK293 cells transfected with scramble or TLK2 shRNA. Quantitative statistical analysis of relative TLK2 protein levels was performed ($n = 4$ independent experiments). **L** Cell viability of HEK293 cells transfected with scramble or TLK2 shRNA under various ionomycin concentrations was assessed ($n = 3$ independent experiments). All data are presented as means \pm SD, * $P < 0.05$, ** $P < 0.01$, *** $P < 0.001$, **** $P < 0.0001$, "ns" indicate no significant difference ($P \geq 0.05$). Source data are provided in the Source Data file.

protein levels led to about 90% neuronal death, compared to roughly 30% cell death in HEK293 cells with similar TLK2 overexpression (Supplementary Fig. 3C, D). This suggests that neurons are more sensitive to TLK2-induced damage. To evaluate the sensitivity to calcium overload, we compared calcium levels in wild-type primary neurons and HEK293 cells using Fluo4-AM, a cell-permeable calcium ion indicator, in response to 1 μM ionomycin. Although neurons exhibited higher baseline fluorescence, ionomycin treatment caused a similar increase in fluorescence in both neurons and HEK293 cells (Supplementary Fig. 3E). However, cell death was more pronounced in neurons than in HEK293 cells (Fig. 3A, B, black lines). Pre-treatment with PMZ reduced cell death in both cell types (Fig. 3A, B, blue lines). In contrast, post-treatment with PMZ, 48 hours after ionomycin addition, decreased cell death in HEK293 cells but had no effect on neurons (Fig. 3A, B, red lines). These findings suggest that postmitotic neurons are more susceptible to calcium overload-induced damage than proliferative cells.

Expression of the NE marker protein Sun1-GFP revealed that NE damage caused by hypoxia-induced calcium overload was rapidly repaired in HEK293 cells (Fig. 3C). In contrast, the same condition in primary cultured neurons resulted in persistent NE damage, which continued until cell death (Fig. 3D). However, pre-treatment with PMZ prevented NE damage in neurons (Fig. 3D). These findings suggest that, while proliferating cells are capable of repairing NE damage, primary neurons lack the ability to effectively repair such damage.

Gain-of-function of TLK2 through either overexpression or calcium overload induces mitotic catastrophe before cell death

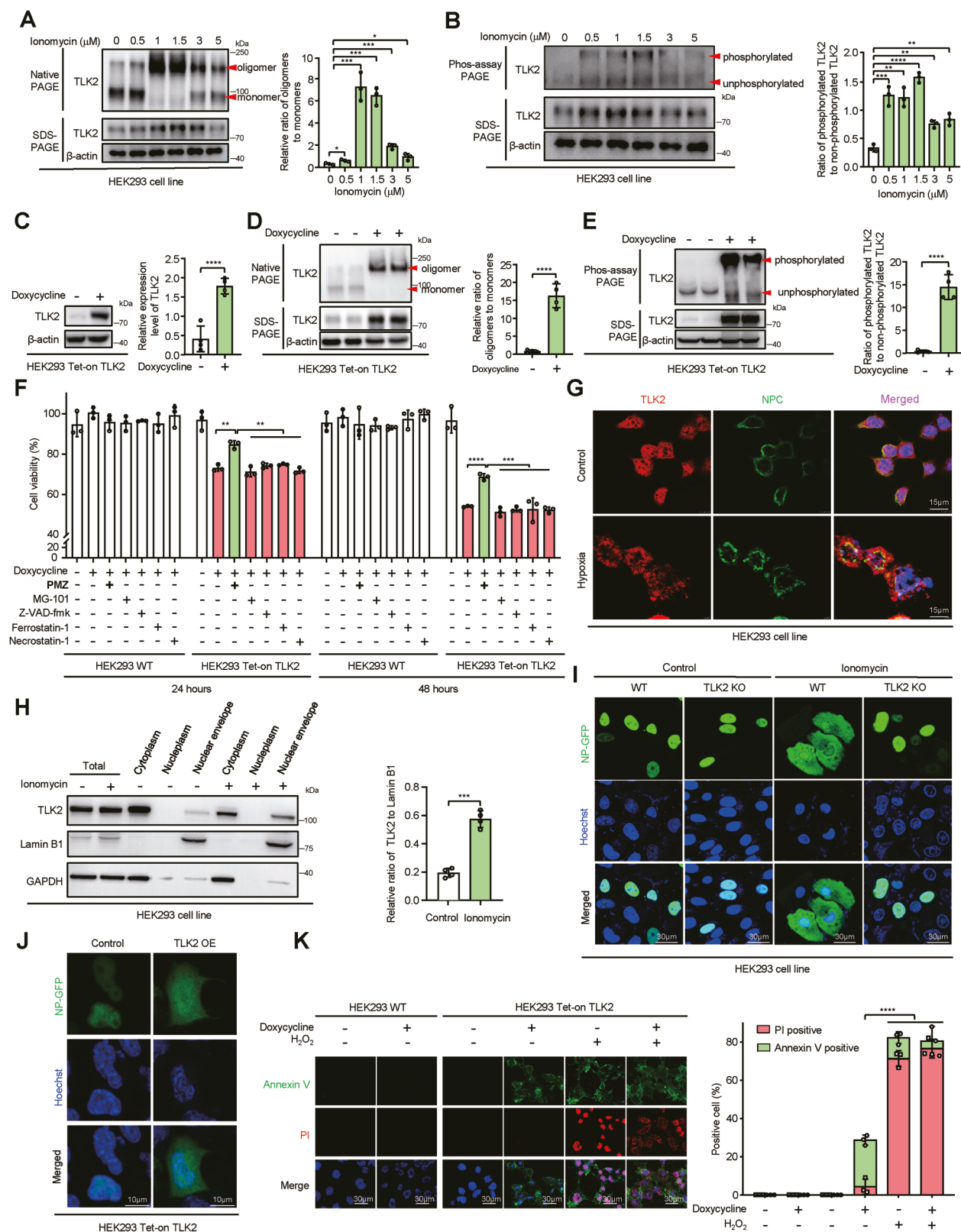
Following TLK2 overexpression, the initial change observed was an increase in nuclear size, a phenomenon known as endomitosis (Fig. 4A). This was subsequently followed by the formation of multinucleated cells, mitochondrial swelling, and ultimately, cell death (Fig. 4B). These morphological changes are similar to cell cycle reentry (CCR) in postmitotic neurons, which is triggered by DNA damage²⁰. To investigate the role of calcium in this process, we utilized the genetically encoded calcium indicator jRCaMP7c. In the G phase of the cell cycle, TLK2-overexpressing cells exhibited low basal calcium levels (Fig. 4C white arrows). However, once the cells entered mitosis, calcium levels were significantly elevated (Fig. 4D red arrows). This calcium elevation, observed during the G1 to S phase transition, has been previously reported²¹. To further support this, quantitative PCR analysis revealed that genes involved in mitosis activation were significantly upregulated in TLK2-overexpressing cells (Supplementary Fig. 4A–E).

Next, we investigated whether calcium overload could trigger CCR in primary cultured neurons. To do this, we performed 5-ethynyl-2-deoxyuridine (EdU) staining, which incorporates into DNA during DNA synthesis²². After treating primary neuron cultures with 1 μM ionomycin, we observed an increase in EdU-positive cells, suggesting that calcium overload triggered CCR (Fig. 4D). Co-staining with the neuron marker NeuN and the cell CCR marker Cyclin D1 confirmed that neurons had re-entered the cell cycle under calcium overload conditions (Fig. 4E). Over time, the number of EdU-positive cells decreased significantly compared to untreated control cells (Supplementary Fig. 4F), indicating that while neurons initiated CCR in response to calcium overload, they eventually undergo cell death. Our findings suggest that TLK2 overexpression, driven by calcium overload, leads to mitotic catastrophe and cell death. The elevation of intracellular calcium levels during mitosis enhances TLK2 activity, contributing to aberrant mitosis and cell death.

TLK2 forms a complex with LC8 and Myosin IIA to promote NE rupture

We used an eye-specific promoter (*GMR-Gal4*) to drive *UAS-TLK* expression (*GMR > TLK*) in *Drosophila* to screen for modifiers of TLK⁹. After screening approximately 4,000 UAS-RNAi lines targeting different genes, we found that an LC8 RNAi line could rescue TLK-mediated cell death (Fig. 5A). LC8 belongs to the dynein light chain family and primarily functions as a hub to promote heterodimer formation²³. In mammalian cells, recombinant TLK2-Flag co-immunoprecipitated with LC8, and ionomycin treatment enhanced their interaction (Fig. 5B). Under LC8 shRNA conditions, TLK2 gain of function induced cell death was alleviated (Fig. 5C, D), indicating that mammalian LC8 is conserved with its fly homolog.

To investigate other potential regulators downstream of TLK2, we performed immunoprecipitation using recombinant TLK2-Flag. Under calcium overload conditions, a protein that binds to TLK2 was identified as the heavy chain of non-muscle myosin IIA through mass spectrometry analysis, and its identity was confirmed by Western blot (Supplementary Fig. 5A, B and Fig. 5E). Myosin IIA is a motor protein that moves along the actin cytoskeleton²⁴. Its tail domain contains multiple phosphorylation sites that regulate its mobility²⁵. We determined its function in cell death by using blebbistatin, an inhibitor of myosin IIA²⁶, which inhibited TLK2 overexpression-induced cell death in a dosage-dependent manner (Fig. 5F). This indicates that myosin IIA plays a functional role in cell death. We then tested whether LC8 acts as a hub to promote interaction between TLK2 and myosin IIA. Under LC8



knockdown, the interaction between TLK2 and myosin IIA was significantly reduced, while LC8 overexpression enhanced its interaction (Fig. 5G).

Based on these results, we propose a hypothesis regarding TLK2/LC8/myosin IIA in nuclear envelope (NE) rupture (Fig. 5H). Calcium overload promotes TLK2 phosphorylation, and activated TLK2 accumulates on the NE. LC8 promotes myosin IIA binding with TLK2 at the

nuclear pores. TLK2 phosphorylates myosin IIA, enhancing its motor function, leading myosin IIA to mobilize on actin and rupture the NE.

To test this hypothesis, we used stimulated emission depletion microscopy (STED) for super-resolution imaging. Compared to the control, ionomycin treatment or TLK2 overexpression increased colocalization of myosin IIA with the nuclear pore complex (Fig. 5I). We observed nuclear pore complexes located away from the nuclear

Fig. 2 | TLK2-mediated cell death is kinase activity-dependent and results in nuclear envelope rupture. **A** Native PAGE analysis was performed to assess the oligomeric and monomeric forms of TLK2 protein in HEK293 cells exposed to varying ionomycin concentrations (0, 0.5, 1, 1.5, 3, 5 μ M), with SDS-PAGE used as a loading control. Quantitative statistical analysis determined the ratio of oligomeric to monomeric forms ($n = 3$ independent experiments). **B** Phos-tag PAGE analysis was conducted to evaluate the phosphorylated and unphosphorylated forms of TLK2 protein in HEK293 cells treated with ionomycin at different concentrations (0, 0.5, 1, 1.5, 3, 5 μ M), using SDS-PAGE as a loading control. A quantitative statistical analysis of the phosphorylated to non-phosphorylated TLK2 ratio was performed ($n = 3$ independent experiments). **C** Western blot analysis was used to assess TLK2 protein expression levels in doxycycline-treated HEK293 Tet-On-TLK2 stable cell lines, with a quantitative analysis of relative TLK2 protein expression ($n = 4$ independent experiments). **D** Native PAGE electrophoresis was performed to analyze the oligomeric and monomeric forms of TLK2 in doxycycline-treated HEK293 Tet-On-TLK2 stable cell lines, with quantitative analysis of the oligomeric to monomeric ratio ($n = 4$ independent experiments). **E** Phos-tag PAGE analysis was used to examine the phosphorylated and unphosphorylated states of TLK2 protein in doxycycline-treated HEK293 Tet-On-TLK2 stable cell lines. A quantitative analysis of the phosphorylated to non-phosphorylated TLK2 ratio was conducted ($n = 4$ independent experiments). **F** Cell death was assessed in doxycycline-treated HEK293 wild-type and Tet-On-TLK2 stable cell lines following exposure to specific concentrations of PMZ, Z-VAD-FMK, Fer-1, and Nec-1 for 24 and 48 hours, respectively ($n = 3$ independent experiments). **G** Representative images of

immunofluorescence staining of TLK2 and the nuclear pore complex in HEK293 cells under normal and hypoxic conditions. Images are representative of three independent experimental replicates. **H** Western blot analysis to determine TLK2 enrichment in nuclear membrane fractions of control and ionomycin-treated groups. LaminB1 was used as a reference control for nuclear membrane components, and GAPDH for cytoplasmic components. A quantitative analysis of TLK2 expression, normalized to LaminB1, was performed ($n = 4$ independent experiments). **I** Representative live-cell imaging was used to track the localization of GFP-fused nucleoplasm in wild-type and TLK2 knockout (KO) HEK293 cell lines, in the presence and absence of ionomycin. Images are representative of three independent experimental replicates. **J** Representative live-cell imaging showing the localization of GFP-fused nucleoplasm in HEK293 cell lines with normal and overexpressed TLK2 levels. Images are representative of three independent experimental replicates. **K** Images of immunofluorescence staining for Annexin V and Propidium Iodide (PI) in HEK293 wild-type and Tet-On-TLK2 stable cell lines, with and without doxycycline treatment. H_2O_2 treatment served as a positive control for PI staining. Images are representative of three independent experimental replicates. A quantitative analysis of the percentage of Annexin V and PI-positive cells under the specified treatments, with and without doxycycline, was performed in both wild-type and Tet-On-TLK2 stable cell lines ($n = 3$ independent experiments). All data are presented as means \pm SD, * $P < 0.05$, ** $P < 0.01$, *** $P < 0.001$, **** $P < 0.0001$, “ns” indicate no significant difference ($P \geq 0.05$). Source data are provided in the Source Data file.

region (Supplementary Fig. 5C), indicating that ruptured NE was pulled away from the nucleus. Additionally, TLK2, LC8, and myosin IIA aggregation increased in the nuclear membrane fraction under ionomycin treatment in a dosage-dependent manner (Supplementary Fig. 5D). The interactions between TLK2/LC8 and TLK2/myosin IIA also increased during calcium overload (Fig. 5E, G). In vitro kinase assays showed that myosin IIA is a substrate of TLK2 (Supplementary Fig. 5E). Together, these studies indicate that TLK2 mediates a type of cell death characterized by ruptured NE, enlarged nucleus, presence of multiple nuclei, and intact plasma membrane. TLK2 is necessary and sufficient for executing this cell death, which we named calcium-induced TLK2-mediated cell death, CaToptosis.

CaToptosis involves in RGC death in mouse models of glaucoma

We generated a conditional knockout of TLK2 using the Cre-loxP recombination system. Two loxP sites flanking exon 4 of TLK2 were engineered using the CRISPR/Cas9 technique (Fig. 6A). To enhance viral expression efficiency, scAAV2-Cre, containing a CMV promoter-driven Cre in a self-complementary adeno-associated virus 2 (scAAV2) expression cassette, was used²⁷. Seven days after intravitreal injection of scAAV2-Cre, TLK2 protein levels were significantly reduced (Supplementary Fig. 6A). Intravitreal injection of N-methyl-D-aspartate (NMDA) in rodents induces calcium toxicity and is a recognized model of normal tension glaucoma²⁸. Studies have shown that NMDA injections ranging from 80 nmol to 320 nmol cause a dose-dependent increase in retinal cell death 7 days post-injection²⁹. Even 10 nmol of NMDA can induce calcium toxicity and retinal ganglion cell (RGC) death within 2 months³⁰. Therefore, NMDA injection dosage can lead to excitotoxicity or calcium overload. We tested NMDA dosages of 10 nmol, 20 nmol, and 30 nmol, assessing RGC survival using Tuj1 (a neuronal marker) and RBPMS (an RGC marker that labels axons and cell bodies)³¹. We found that 10 nmol NMDA was sufficient to induce 80% RGC death 7 days after injection, with higher dosages causing more extensive RGC death (Supplementary Fig. 6B). In the conditional TLK2 knockout scenario, the expression efficiency of 3xFlag-Cre determined the number of affected RGCs. Seven days after scAAV2-3xFlag-Cre injection, over 90% of RGCs expressed the Flag tag (Supplementary Fig. 6C). Following 10 nmol NMDA application, RGC death was significantly reduced in the TLK2 knockout background compared to control mice (Fig. 6B). However, the protective effect was weaker with 30 nmol NMDA administration (Fig. 6B). This suggests that TLK2

knockout may preferentially inhibit calcium overload-induced death (10 nmol NMDA). The optic nerve crush (ONC) model is also known to induce calcium overload in RGCs³².

In wild-type mice, prominent RGC death was observed 7 days post-operation. In contrast, RGC death was significantly reduced in TLK2 knockout mice (Fig. 6C).

To investigate the effects of TLK2 gain-of-function in vivo, we examined mice with conditionally expressed TLK2 (Supplementary Fig. 3A). Seven days after injecting scAAV2-Cre into the eye, over 90% of retinal ganglion cells (RGCs) expressed Cre (Supplementary Fig. 6D). Following 3 weeks of TLK2 overexpression induced by Cre, there was a significant reduction in RGCs compared to wild-type mice (Supplementary Fig. 6E). This demonstrates that TLK2 gain-of-function is sufficient to cause RGC death in mice.

To test the therapeutic potential of targeting TLK2, we constructed a scAAV2-shTLK2 vector (Fig. 6D) and validated its knockdown effect in HEK293 cells (Supplementary Fig. 6F). The knockdown effect of scAAV2-shTLK2 in the retina was confirmed (Supplementary Fig. 6G). In the NMDA-induced model (10 nmol NMDA), RGC survival was approximately 60% in scAAV2-shTLK2 pre-infected retinas, compared to 20% in the control group (Fig. 6E). In the ONC model, RGC survival was nearly 30% in control mice but almost 90% with scAAV2-shTLK2 treatment (Fig. 6F).

To investigate the impact of TLK2 knockdown on RGC axon survival, we administered Alexa Fluor 488-conjugated Cholera Toxin Subunit B (CTB) to mice in the NMDA model to observe CTB distribution within the optic nerve (Fig. 6G). One week post-NMDA injection, RGC axons were severely compromised, with a marked reduction in CTB green fluorescence intensity compared to the undamaged control group (Fig. 6G). In contrast, following shTLK2 treatment, most axons were protected from NMDA damage, and CTB green fluorescence intensity was preserved (Fig. 6G). In the visual water maze, mice were trained to swim towards low spatial frequency gratings, with the frequency gradually increasing. The spatial frequency threshold was determined when the mice made fewer than 70% correct choices³³. The visual acuity of uninjured mice was 0.6 cycles per degree (c/d), which dropped to 0.185 c/d after NMDA damage. Notably, silencing TLK2 significantly improved spatial acuity to 0.355 c/d (Fig. 6H). Collectively, our data suggest that targeting TLK2 may be an effective strategy to prevent RGC death and preserve visual function.

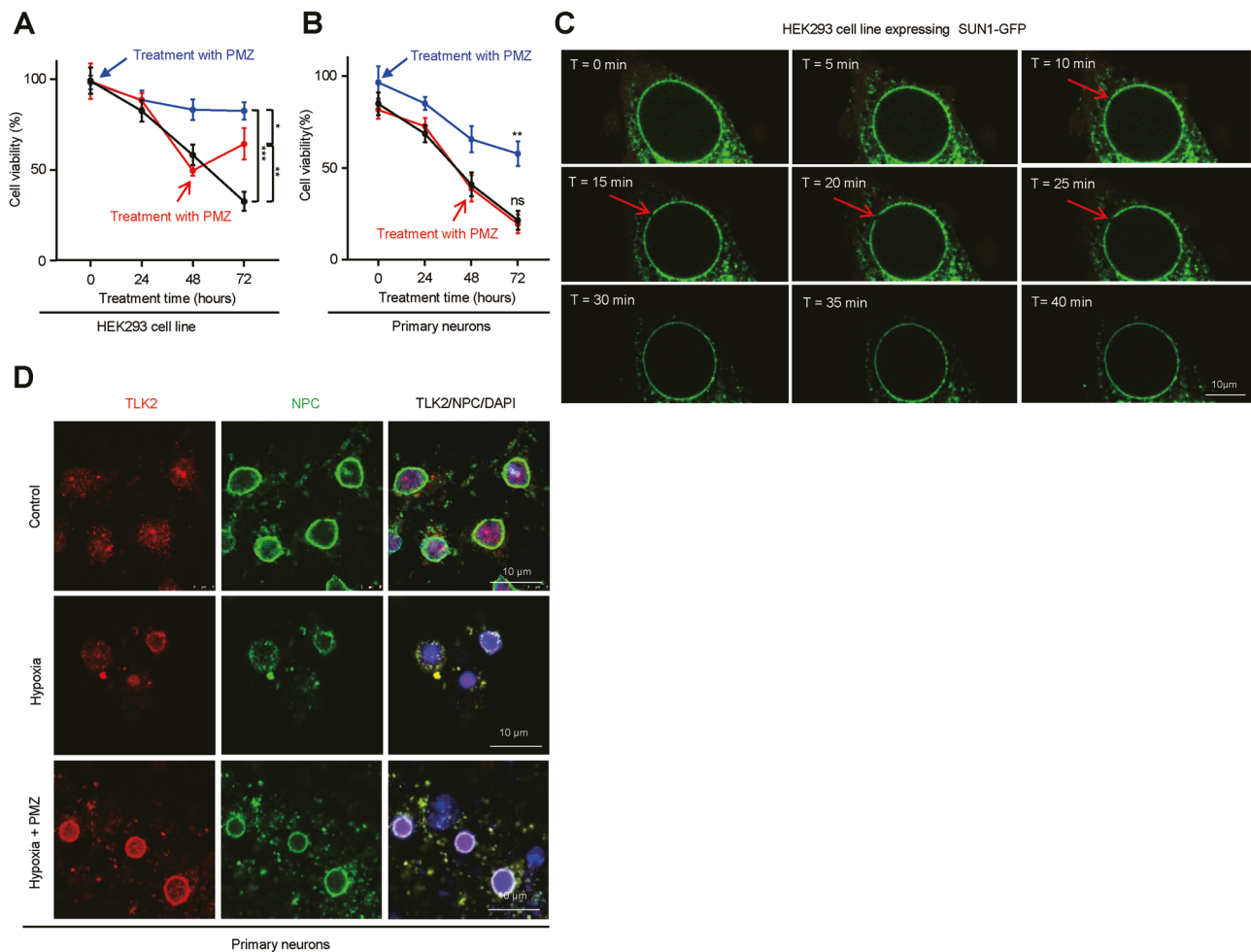


Fig. 3 | Compared with primary neurons, proliferating cells can repair the nuclear membrane to reduce cell death caused by calcium overload. **A** Cell viability was assessed in HEK293 cell lines following treatment with 1 μ M ionomycin at different time intervals after PMZ addition (0 h, represented by the blue line, and 48 h, represented by the red line) ($n = 3$ independent experiments). **B** Cell viability was assessed in primary cultured neurons following the same treatment regimen (1 μ M ionomycin) at varying time intervals post-PMZ addition (0 h, blue line; 48 h, red line) ($n = 3$ independent experiments). **C** Images from live-cell imaging of HEK293 cells transfected with the nuclear membrane protein SUN1-GFP were

captured to observe the integrity of the nuclear membrane following 1 μ M ionomycin treatment. The red arrow indicates nuclear envelope rupture. Images are representative of three independent experimental replicates. **D** Images of immunofluorescence staining of TLK2 and the nuclear pore complex in primary cultured neurons, comparing normal and hypoxic conditions, with and without PMZ treatment. Images are representative of three independent experimental replicates. All data are presented as means \pm SD, ** $P < 0.01$, *** $P < 0.001$, “ns” indicate no significant difference ($P \geq 0.05$). Source data are provided in the Source Data file.

We further determined whether NMDA treatment could promote cellular features of CaToptosis, including CCR and NE rupture in RGCs. Four days after NMDA (10 nmol) injection, we observed nearly 14% of RGCs were positively stained by EdU (Fig. 6I). To determine NE rupture, we infected AAV2 to express Np-GFP for one month, resulting in approximately 20% RGC labeling. Four days after NMDA (10 nmol) injection, we observed GFP spread throughout the entire cell in some RGCs (Fig. 6J). These data indicate that CaToptosis occurs in vivo.

Discussion

Although the terms calcium overload and excitotoxicity are often used interchangeably, they refer to distinct cellular conditions. Calcium overload is characterized by a mild disturbance in intracellular calcium levels, allowing neurons to survive over extended periods—a phenomenon observed in brain aging and slow-progressing neurodegenerative disorders³⁴. For example, in Alzheimer’s disease models, mitochondrial calcium concentrations can reach up to 1.6 μ M before neuronal death occurs³⁵. In contrast, excitotoxicity involves severe elevations of intracellular calcium, leading to rapid neuronal death, as seen in acute ischemic stroke³⁶. While biomarkers for excitotoxicity,

such as calpain and cathepsin activation, are well-established³⁷, robust markers for calcium overload are lacking.

We propose that gain-of-function in TLK2, which include increased protein level, multimer formation and phosphorylation, may serve as a biomarker for calcium overload. These features distinguish calcium overload from calpain activation, which is often used as a marker of excitotoxicity. In our experiments using HEK293 cells and primary neuron cultures, we observed a 3.3- to 4-fold increase in $[Ca^{2+}]_i$ from baseline, which we consider indicative of calcium overload. This range of calcium increase is consistent with findings from other studies demonstrating that overexpression of proteins such as α -synuclein or amyloid-beta ($A\beta$) peptides can similarly elevate $[Ca^{2+}]_i$ by 2- to 4-fold, as measured using Fura-2 or ratiometric calcium indicators like Yellow Cameleon^{35,38,39}. In contrast, excitotoxic stress, such as that induced by glutamate treatment, has been shown to elevate $[Ca^{2+}]_i$ from 5.9- to 16.9-fold. This aligns with previous reports indicating that glutamate-induced excitotoxicity can elevate $[Ca^{2+}]_i$ to levels between 5–10 μ M, a range associated with neuronal cell death⁴⁰.

According to the Nomenclature Committee on Cell Death, the classification of cell death should be based on molecular mechanisms

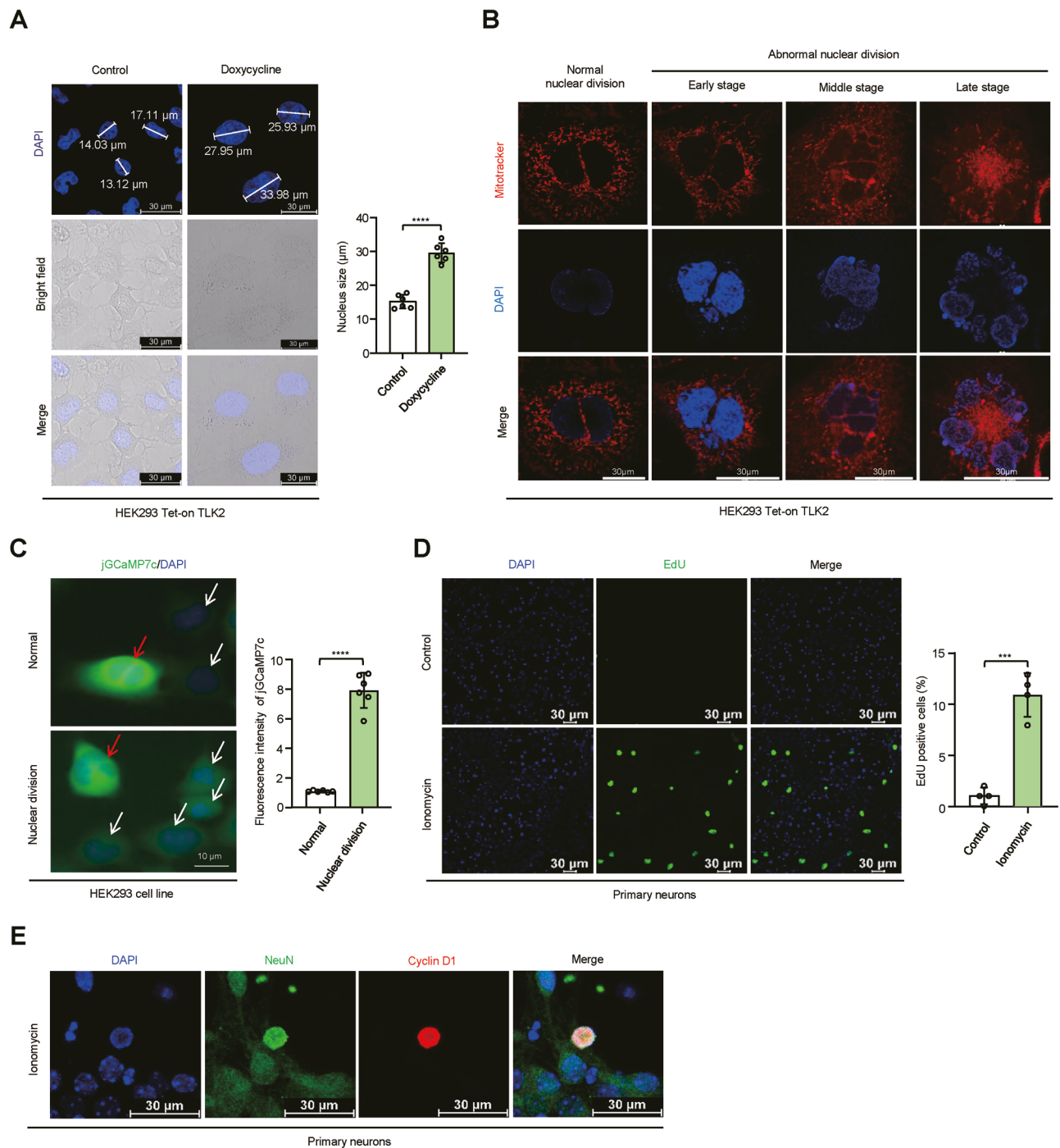
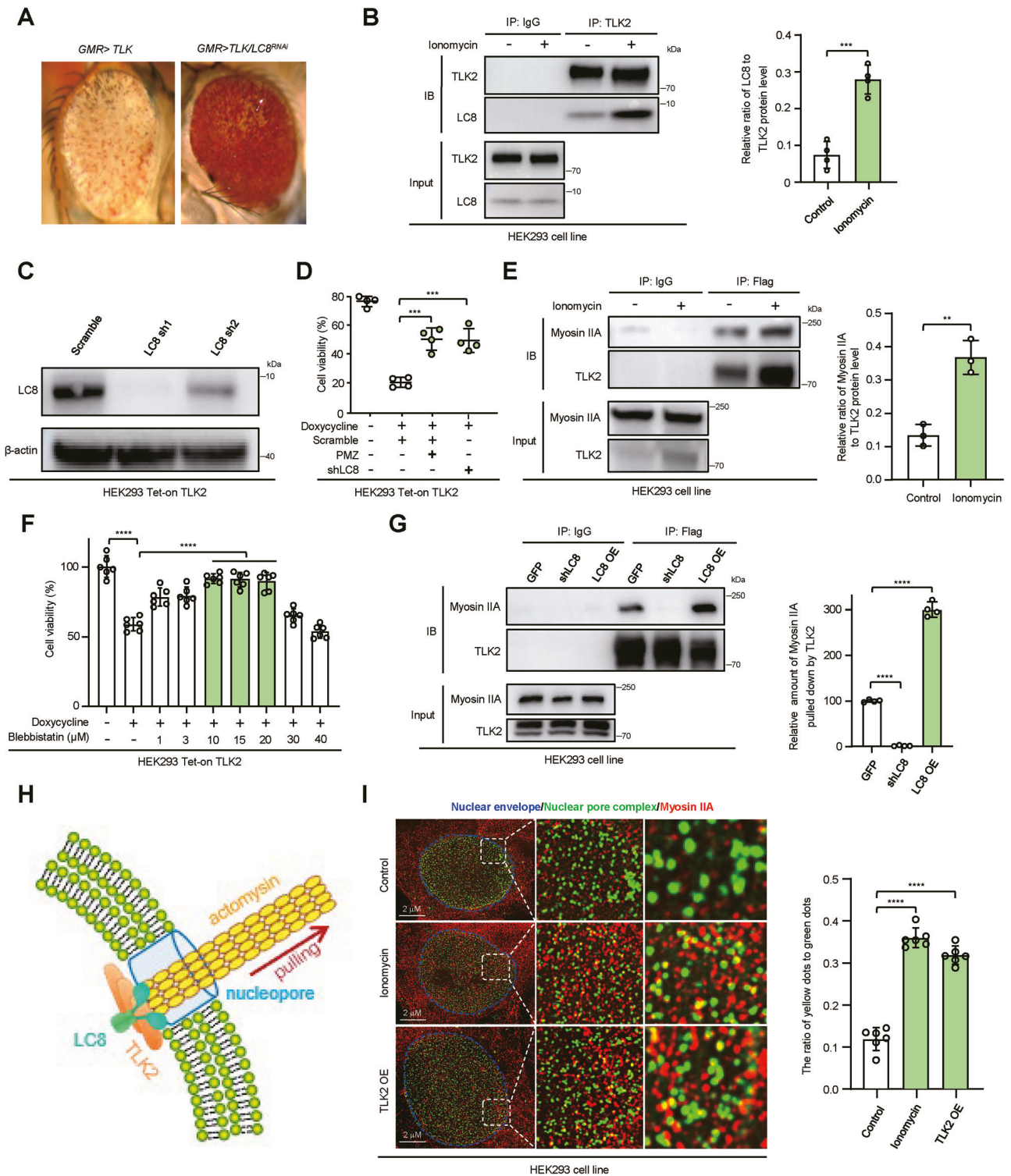


Fig. 4 | TLK2 can lead to abnormal division of proliferating cells and cause neurons to re-enter the cell cycle. **A** Quantitative assessment of nuclear size in HEK293 cells under normal conditions and following doxycycline-induced overexpression of TLK2. Images are representative of three independent experimental replicates. Nuclear dimensions were measured using the Leica SP8 imaging system and LAS X software. A comprehensive quantitative analysis of nuclear size parameters was then performed to evaluate the impact of TLK2 overexpression ($n = 7$ cells from 3 independent experiments). **B** Images of nuclear morphology (stained with DAPI, blue) and mitochondrial morphology (stained with Mitotracker, red) were obtained in Tet-on TLK2 HEK293 cells following doxycycline treatment for various durations. The images highlight different stages of cellular morphological changes for reference. Images are representative of three independent experimental replicates. **C** Images of live-cell imaging showing the green fluorescence intensity of jGCaMP7c in HEK293 cells under normal conditions (indicated by white

arrows) and conditions with aberrant nuclear division (indicated by red arrows). Images are representative of three independent experimental replicates. Analysis of fluorescence intensity was conducted to compare the two conditions ($n = 6$ cells from 3 independent experiments). **D** Immunofluorescence detection of EdU incorporation was used to assess cell proliferation in primary cultured neurons, both with and without ionomycin treatment. Images are representative of three independent experimental replicates. The proportion of EdU-positive cells, indicative of active DNA synthesis, was quantified to evaluate the effects of ionomycin on proliferation ($n = 4$ independent experiments). **E** Confocal microscopy images of primary cultured neurons treated with ionomycin, co-immunostained with NeuN, cyclin D1, and DAPI, are shown. Images are representative of three independent experimental replicates. All data are presented as means \pm SD, *** $P < 0.001$, **** $P < 0.0001$, “ns” indicate no significant difference ($P \geq 0.05$). Source data are provided in the Source Data file.



rather than morphological characteristics¹⁹. Calcium overload is known to initiate various death signals, including autophagy failure, mitochondrial dysfunction, and NE rupture. However, analyzing calcium overload alone does not fully elucidate the molecular pathways underlying TLK2-induced cell death. Using an inducible TLK2 expression cell line, we observed hallmark features of calcium overload, such as NE rupture and CCR preceding cell death. These findings highlight TLK2's crucial role in driving neuronal degeneration. Our results show that TLK2, LC8, and myosin II form a complex at the NE, which may lead to NE rupture. Further investigation is needed to clarify the

precise mechanism. We propose naming this calcium overload-induced, TLK2/LC8/myosin II-mediated cell death pathway “CaTopsis.”

Calcium overload is also associated with CCR, a pathological hallmark commonly observed in the aging brain⁴¹. Single-nucleus RNA sequencing studies indicate that approximately 10% of neurons in AD brains exhibit CCR markers—a rate significantly higher than in healthy brains⁴². Postmortem analyses have revealed that up to 90% of neuronal deaths in AD display signs of CCR^{43,44}. Excessive calcium influx, particularly through NMDA receptors, can trigger this aberrant CCR⁴⁵.

Fig. 5 | TLK2 forms a complex with LC8 and Myosin IIA to promote NE rupture.

A Eye phenotype of *Drosophila* expressing *UAS-TLK* driven by *GMR-Gal4* (*GMR* > *TLK*) after crossing with scramble strain (left) and TLK2 RNAi strain (right). Images are representative of three flies with the indicated genotypes.

B Immunoprecipitation using Flag antibody in HEK293T cells transfected with 3×Flag-TLK2 protein, under normal and 1 μM ionomycin-treated conditions. Blotting with LC8 antibody and quantification of relative LC8 to TLK2 protein ratio ($n = 4$ independent experiments). **C** Western blot analysis of LC8 protein expression levels in HEK293 cells following transfection with scramble shRNA and LC8 shRNA, and quantitative statistical analysis of LC8 protein levels. Images are representative of three independent experimental replicates. **D** Cell survival was assessed in HEK293 Tet-On-TLK2 stable cell lines treated with or without doxycycline, PMZ, scramble shRNA, and LC8 shRNA ($n = 4$ independent experiments). **E** Co-immunoprecipitation of TLK2 and Myosin IIA was conducted in HEK293T cells with or without ionomycin treatment. Immunoprecipitation was performed using Flag-M2 antibody to selectively pull down Myosin IIA ($n = 3$ independent experiments).

F Cell survival of HEK293 tet-on-TLK2 stable cell line treated with doxycycline and various concentrations of Blebbistatin (0, 1, 3, 10, 15, 20, 30, and 40 μM) ($n = 6$ independent experiments). **G** Co-immunoprecipitation experiments utilizing a Flag antibody in HEK293T cells overexpressing the 3×Flag-TLK2 protein, in the presence of a GFP plasmid, LC8 knockdown shRNA plasmid, and recombinant LC8 plasmid. Detection and quantification of Myosin IIA protein and the TLK2-Myosin IIA binding affinity ($n = 4$ independent experiments). **H** Schematic of TLK2, LC8, and Myosin IIA enrichment on the nuclear envelope. Created in PowerPoint. **I** Colocalization analysis of the nuclear pore complex (green) and Myosin IIA (red) was performed in normal cells (top), ionomycin-induced calcium overload cells (middle), and TLK2-overexpressing cells (bottom) using STED microscopy. The rightmost column shows enlarged images highlighting the colocalization of Myosin IIA with the nuclear pore complex (yellow dots). Quantitative analysis of colocalization is represented by the yellow/green dot ratio ($n = 6$ cells form 3 independent experiments). All data are presented as means ± SD, ** $P < 0.01$, *** $P < 0.001$, **** $P < 0.0001$. Source data are provided in the Source Data file.

Notably, memantine, an NMDA receptor inhibitor, can prevent CCR and ameliorate Alzheimer's disease symptoms in mouse models⁴⁶. Our research identifies a molecular link between calcium overload and CCR, suggesting that calcium overload enhances the TLK2/LC8/myosin II complex, thereby exacerbating CCR. Importantly, TLK2-induced CCR appears to diverge mechanistically from normal mitosis. Under physiological conditions, NE disassembly during mitosis is driven by cyclin-dependent kinase-mediated phosphorylation of inner nuclear membrane proteins⁴⁷. In *Drosophila*, TLK has been implicated in the G2/M transition, where it cooperates with ASF1 to regulate mitotic spindle assembly and chromatin dynamics⁴⁸. However, our data show that TLK-induced cell death does not depend on ASF1, suggesting an alternative mechanism⁹. Supporting this, TLK2 overexpression upregulates key CCR regulators. Interestingly, calcium signaling plays a crucial role in NE breakdown during normal mitosis, with myosin II facilitating actin cortex contraction⁴⁹. This suggests that physiological calcium waves are crucial for mitosis. In contrast, under conditions of calcium overload or TLK2 overexpression, this calcium wave becomes pathological, particularly in postmitotic neurons. Although we did not manipulate the TLK2/LC8/myosin II pathway to directly evaluate its role in CCR regulation, this represents an intriguing avenue for future research.

The Nomenclature Committee on Cell Death has recommended against classifying mitotic catastrophe as a distinct form of cell death due to its variable outcomes⁵. In contrast, our data demonstrate that proliferating cells are capable of repairing NE damage induced by calcium overload, a repair mechanism that appears to be absent in neurons. These findings suggest that CaToposis, a form of cell death triggered by calcium overload, is a unique stress response specific to neurons and warrants recognition as a distinct form of cell death. We have identified key molecular mechanisms and biomarkers associated with calcium overload in neurons. Moreover, our successful targeting of TLK2 to protect retinal ganglion cells in mouse models of glaucoma further supports the in vivo relevance of CaToposis, indicating that it plays a significant pathological role in neurodegenerative conditions.

Methods

Drosophila stock and maintenance

Drosophila stocks were maintained at 25 °C on standard fly food. TRiP (Transgenic RNAi Project) RNAi stocks were obtained from the Tsinghua *Drosophila* stock center (Beijing, China). The TRiP RNAi lines were inserted in a known genomic region on the left arm of 2nd chromosome (25C6) or the left arm of 3rd chromosome (68A4). These sites are known to provide high level expression of the transgene⁵⁰. TB00072 (BL36303) was used as a genetic background matched control. The *UAS-Pgk* line was generated by our own, and had published previously.

Mouse maintenance

Male C57BL/6J mice (8 weeks old) were purchased from the Vital River Laboratory Animal Technology (Beijing, China). Animals were housed under a 12 h light/dark cycle with free access for food and water. All experiments using mice and rats were approved by the Institutional Animal Care and Use Committee, Capital Medical University (Approval NO: AEEI-2021-123).

TLK2 conditional overexpression mice

Using homologous recombination, ES cell targeting was employed to insert the CAG-3Xstop-TLK2-polyA cassette at the H11 locus. The primer sequences for constructing the targeting vector were as follows:

Mir-122-1 CGCGGTACCAAACCATGACGAGGTGAG

Mir-122-2 GCTCTAGATGGGTGTCAGGGTAGTCA

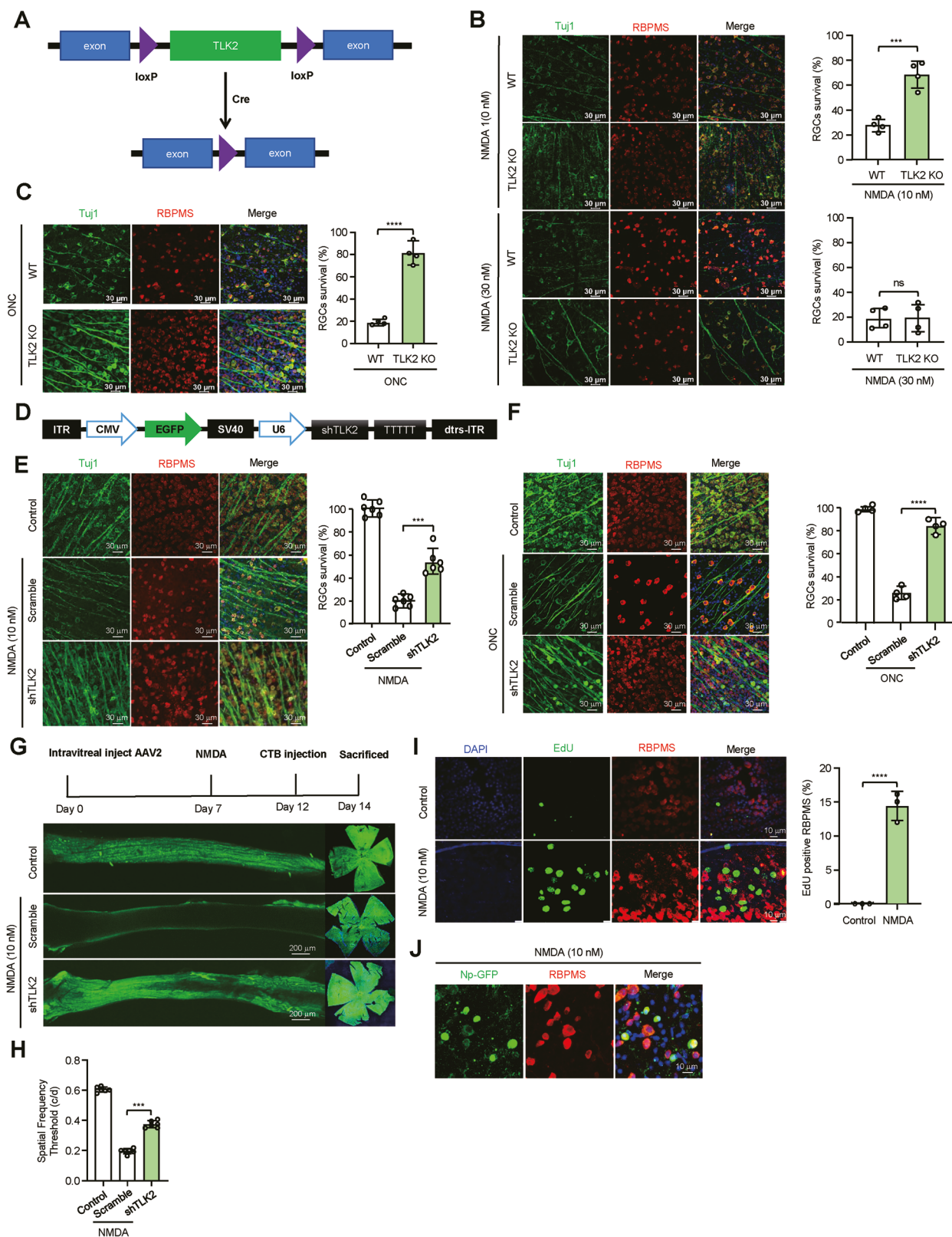
After obtaining homozygous TLK2CKI/CKI mice, retinal-specific overexpression of TLK2 was achieved via intravitreal injection of scAAV2/2-CMV-CRE virus.

TLK2 knockout mice

TLK2 knockout mice were also purchased from Shanghai Model Organisms Center. The Cre-lox system was used for the deletion of TLK2 gene (ENSG00000146872). TLK2^{flx/flx} mice were generated by CRISPR-Cas9 technology which targeted exon4. TLK2 genes could be knocked out ubiquitously by Intravitreal injection of scAAV2/2-CMV-cre virus.

Cell culture studies

HEK293T cells (human embryonic kidney cells) and HEK293 cells (human embryonic kidney cells) were obtained from the American Type Culture Collection. The culture medium used was DMEM complete medium (with 10% fetal bovine serum and 1% penicillin-streptomycin). The cells were passaged at a ratio of 1:3 with a passaging density of 90%. Mycoplasma testing was performed, and the results were negative. Primary mouse neurons: To prepare embryonic mouse (E18) cortical neurons, the cortical brain tissue was removed and placed in ice-cold DMEM (Dulbecco's Modified Eagle Medium) (Gibco, USA). The meninges were removed, and the tissue was transferred to 5 ml of 0.25% trypsin dissociation medium. The tissue was finely chopped and incubated with continuous shaking at 37 °C for 10-20 minutes. Digestion was terminated with DMEM containing 10% fetal bovine serum, and the mixture was triturated using a 10 ml pipette. Undigested tissue was allowed to settle at the bottom of the tube, and the supernatant was collected into a sterile screw-cap tube and centrifuged at 130 g for 5 minutes at room temperature. The supernatant was discarded, and the cell pellet was resuspended in DMEM containing 10% fetal bovine serum (Gibco, USA) and 0.25% penicillin-streptomycin (Invitrogen, USA). Cells were filtered using a 40 μm cell



filter (BD Falcon, USA). Cells were then plated on poly-L-lysine-coated dishes and maintained in neurobasal medium containing B27 supplement (Invitrogen, USA), glutamine (Invitrogen, USA), and penicillin (Invitrogen, USA). After 48 hours of culture, 10 μM cytarabine was added to the medium for 24 hours to inhibit glial cell proliferation.

Measurement of intracellular calcium concentration using the Fura-2 fluorescence assay

The intracellular calcium concentration was measured using the Fura-2 fluorescence assay as follows. Cell preparation, cells were seeded onto black, transparent-bottom 96-well microplates and cultured until approximately 70% confluence. They were then washed with Hank's

Fig. 6 | TLK2 plays a critical role in retinal ganglion cell death in glaucoma models. **A** Schematic representation of the TLK2 conditional knockout (CKO) mouse model. **B** Confocal microscopy images showing the survival of retinal ganglion cells (RGCs) in wild-type and TLK2 CKO transgenic mice, double-labeled with Tuj1 and RBPMS, following intravitreal injection of sc-AAV2/2-CMV-Cre virus. Mice were intravitreally injected with 10 nmol and 30 nmol NMDA, and RGC survival rates were assessed ($n = 4$ retinas from 4 mice per indicated genotype). **C** Quantification of RGC survival in wild-type and TLK2 CKO transgenic mice treated with optic nerve crush (ONC), showing corresponding survival rates of RGCs ($n = 4$ retinas from 4 mice per indicated genotype). **D** Diagram illustrating the design of the self-complementary double-stranded AAV2/2 (scAAV2/2) vector, driven by the U6 promoter, expressing shTLK2 for TLK2 knockdown. **E** Confocal images showing RGC survival in NMDA-injected mice. RGCs were labeled with RBPMS in wild-type and TLK2 CKO mice following intravitreal injection of sc-AAV2/2-CMV-Cre virus. Corresponding RGC survival rates are presented ($n = 6$ retinas per group). **F** Confocal images showing RGC survival in the ONC model, including control

(normal mouse retina), scramble (mice injected with scrambled shRNA), and shTLK2 (mice injected with TLK2 knockdown virus) groups. Survival rates of RGCs are shown for each treatment ($n = 4$ retinas per group). **G** Schematic representation of the experimental protocol for scAAV2/2 injection, glaucoma model induction, and cholera toxin B (CTB) injection. Confocal images display the fluorescence intensity of CTB-Alexa Fluor 488 conjugate in optic nerves of mice treated with NMDA and NMDA + shTLK2. Images are representative of three independent experimental replicates. **H** Statistical analysis of visual acuity in mice assessed by the visual water maze test. ($n = 6$ mice per group). **I** Confocal images showing EdU, RBPMS, and DAPI staining in the retina of mice following NMDA treatment ($n = 3$ independent experiments). **J** Confocal image showing Np-GFP, RBPMS, and DAPI staining in the retina of mice following NMDA treatment. Images are representative of three independent experimental replicates. All data are presented as means \pm SD, *** $P < 0.001$, **** $P < 0.0001$, "ns" indicate no significant difference ($P \geq 0.05$). Source data are provided in the Source Data file.

Balanced Salt Solution (HBSS) without calcium and magnesium. They are then washed with Hank's Balanced Salt Solution (HBSS) without calcium and magnesium. Dye loading, Fura-2 AM was dissolved in DMSO and combined with Pluronic F-127 to improve cell permeability. The solution was diluted in HBSS and applied to the cells. After incubation for 45 minutes at 37 °C in the dark, excess dye was removed by washing with HBSS containing calcium and magnesium. Fluorescence measurement, fluorescence was measured using a microscope or plate reader by exciting the dye at 340 nm and 380 nm and recording emission at 510 nm. The ratio of fluorescence intensities ($R = 340/380$) was calculated to assess intracellular calcium levels. Calibration values were obtained by determining R_{min} and F_{min} using wells treated with EGTA to chelate calcium. Determining R_{max} and F_{max} using wells treated with 2 mg/mL calcium and ionomycin to saturate calcium levels. The Grynkiewicz equation was used to calculate absolute calcium concentration: where Kd is the dye's dissociation constant, R is the fluorescence ratio, and F_{min} and F_{max} are the minimum and maximum fluorescence intensities at 380 nm, respectively. The intracellular calcium dynamics were visualized by plotting the calculated calcium concentrations over time.

$$[Ca^{2+}] = Kd \times \frac{(R_{max} - R)}{(R - R_{min})} \times \frac{F_{min}}{F_{max}}$$

Construction of Tet-on regulated expression stable cell line

TLK2 (NM_00112705.2) was cloned into the protein-coding region of the FUW-tetO-MCS vector to obtain FUW-tetO-TLK2, which was co-transfected with the regulatory plasmid FUW-M2rtTA and the helper plasmids pCMV-VSVG and pCAG-dR8.9 into HEK293T cells at a molar ratio of 1:1:1 for virus packaging. After 72 hours of viral expression, the virus was collected, purified, and concentrated. Cells to be infected were seeded into 96-well plates and cultured overnight at 37 °C in a 5% CO₂ incubator. Lentiviral infection reagent (polybrene) was added to the cells, followed by the addition of a certain volume of concentrated lentivirus according to the cell MOI. After cells resumed normal proliferation, single clones were isolated using the limiting dilution method into 96-well plates. After one week, visible single clones were selected for expansion. The Tet-on inducible expression system requires the addition of a certain concentration of doxycycline to induce gene expression once the cells reach a certain density. Positive cell clones that could induce gene expression were identified by immunoblotting, followed by expansion and subsequent experiments.

Cell death and cell viability assay

Cell death was assessed using the lactate dehydrogenase (LDH) cytotoxicity assay kit (beyotime, C0016). Cells were seeded in 24-well plates the day before treatment. Cells were cultured with or without

appropriate drugs, and at the designated times, supernatant LDH and total intracellular LDH were measured. For supernatant LDH measurement, 120 μ L of supernatant from each well was transferred to a new 96-well plate, and detection reagent was added for sample measurement. For intracellular LDH measurement, the supernatant was carefully removed, and LDH release reagent was added, followed by gentle shaking and incubation for 1 hour. Then, 120 μ L of supernatant from each well was transferred to a new 96-well plate, and detection reagent was added for sample measurement. The mixture was incubated at room temperature (approximately 25 °C) in the dark for 30 minutes, and absorbance was measured at 490 nm. Cell death was calculated as: supernatant LDH / (supernatant + intracellular LDH) \times 100%. For cell viability, 5000-10000 cells were seeded into each well of a 96-well plate the day before treatment. Each well was then replaced with 100 μ L of fresh medium containing 10% CCK-8 reagent (beyotime, C0043). After 1 hour of incubation, absorbance was measured at 450 nm using a microplate reader. Cell viability was calculated as: (absorbance of treated compound - blank absorbance)/(control absorbance - blank absorbance) \times 100%.

Immunoprecipitation and mass spectrometry

HEK293T cells were transfected with pcDNA3.1-3 \times FLAG-mTLK2 recombinant plasmid, and after 48 hours, cells were scraped and lysed using NP-40 lysis buffer (20 mM Tris pH7.5, 150 mM NaCl, 1% Triton X-100, containing protease and phosphatase inhibitors). 500 μ g of protein was incubated with 3 μ g of mouse FLAG antibody (FLAG[®] BioM2, sigma) or 3 μ g of mouse IgG (sigma, 12-371) control. The EP tubes were placed in a 4 °C shaker overnight. The next day, the antibody-protein complexes were added to pre-washed magnetic beads and incubated for 4 hours with gentle mixing. The antigen-antibody-bead complexes were separated on a magnetic rack, washed four times, and eluted by adding 100 μ L of 1 \times SDS-PAGE sample buffer, vortexed thoroughly, and heated at 95 °C for 10 minutes. The boiled samples were placed on the magnetic rack for 10 seconds to separate the beads, and the supernatant was collected for SDS-PAGE analysis. After SDS-PAGE, the gel was stained with Coomassie Brilliant Blue, and bands were excised for in-gel digestion, followed by mass spectrometry analysis.

Western blotting

Tissues or cells were lysed in lysis buffer (50 mM Tris, 150 mM NaCl, 1% Triton X-100, 1% sodium deoxycholate and 0.1% SDS) supplemented with protease inhibitor cocktail (Roche #11697498001) and PMSF (Beyotime #ST507) for 15 minutes on ice. Then the lysis was sonicated for 2 minute with 50 w (3 s on/3 s off) on ice and centrifugation at 15294 g 4 °C for 15 minutes. Supernatants were collected and boiled with SDS loading buffer at 95 °C for 5 minutes. 10-40 μ g protein from cell lysate or tissue homogenate were loaded on 12% SDS-PAGE gels. Transferring the protein from the gel to the PVDF membrane

(Millipore #ISEQ00010). Membranes were blocked with 5% milk for one hour at room temperature. Primary antibodies to the following proteins were used for western blotting at the indicated concentrations: TLK2(1:1000, proteintech, 13979-1-AP), non-muscle Myosin IIA (1:1000, abcam, ab138498), DYNLL1/PIN (1:1000, abcam, ab51603), β -actin (1:1000, proteintech, 66009-1-Ig), GAPDH (1:1000, proteintech, 60004-1-Ig), caspase-3 (1:1000, CST, 9662), Cleaved caspase-3 (CST, 1:1000, 9661), laminB1(1:1000, abcam, ab16048), γ H2AX (1:1000, abcam, ab229914). Incubated overnight at 4 °C. Washing the membrane 3 times for 5 minutes each with TBST (TBS containing 0.1 % Tween20), and then incubating with HRP secondary antibody (1:10000) for one hour at room temperature. Acquiring image using HRP substrate (Millipore #WBKLS0500) for chemiluminescence with VILBER Fusion FX SPECTRA equipment.

Native-page

Lyse Cells in Lysis Buffer (20 mM Tris, 150 mM NaCl, 10% Glycerol, 1% NP40 and 5Mm Na₃VO₄). Then the lysis was centrifugation at 15294 g 4 °C for 15 minutes, supernatants were collected, add sodium deoxycholate (DOC-Na₂) to final concentration of 0.4%, mix with 5X native loading buffer (125 mM Tris, 960 mM Glycine, 40% Glycerol, 0.005% Bromophenol Blue), do not boiled. Cathod Buffer: 25 mM Tris, 192 mM Glycine, 0.4% DOC-Na₂. Anode Buffer: 25 mM Tris, 192 mM Glycine, without DOC-Na₂. In cold room, 200 V, 70 min, pre-run to current drops to -10 mA per Gel. load sample, move to cold room, 200 V 60 min. Transfer and do Westen blot as usual.

Phos-tag western blot

Cell lysis is performed as described in western blotting, Then the lysis was centrifugation at 15294 g 4 °C for 15 minutes, supernatants were collected, the supernatants were treated with 1 mM MnCl₂ and boiled with SDS loading buffer at 95 °C for 10 minutes. 40 μ mol/L MnCl₂ and 20 μ mol/L phos-tag (Wako #30493521) were added to the SDS-PAGE (8 %). After the electrophoresis, the phos-tag gels were incubating with transfer buffer containing 5 mM EDTA for 20 minutes twice to remove the divalent cations 48. Washing with transfer buffer for 10 minutes once. Transferring the protein from the gel to the PVDF membrane. The next blocking and antibody incubation were the same as the normal western blot procedures.

Purification of protein and kinase assay

The sequences of TLK2 (NM_001294334.1) and Myosin IIA (NM_002473) were synthesized with a 3 \times Flag tag and cloned into the pcDNA3.1-CMV vector for expression in a eukaryotic cell system. The plasmids were transfected into normally cultured HEK293T cells, after which the cells and supernatant were collected (130 g, 5 min). The cells were lysed, and the recombinant protein was separated using Anti-Flag magnetic beads. For every 10 μ L of original bead volume, 100 μ L of 3 \times Flag peptide elution solution (150 μ g/mL) was added. After incubation, the mixture was placed on a magnetic rack for separation, and the supernatant was transferred to a new centrifuge tube. The supernatant contained the eluted Flag-tagged protein, which was stored at 4 °C for immediate use or at -80 °C for long-term storage. A standard kinase assay was performed for 15 minutes at room temperature in 50 μ L of kinase buffer (10 mM Tris pH 7.5, 50 mM KCl, 10 mM MgCl₂, 1 mM DTT) supplemented with 1 μ L ATP (0.2 mM) and 1 μ g of TLK2 purification proteins and 20 μ g substrates MBP (Millipore #13-110) or purified Myosin IIA. The remaining ATP in the sample wells was measured based on a standard curve to calculate enzyme activity.

Annexin V/PI staining

Seed the cells in a confocal dish, treat with drugs, and collect the cells. Wash the cells with fresh PBS. Add Annexin V Alexa Fluor[®] 488 to 1 \times Annexin binding buffer at a ratio of 20:1 and propidium iodide (PI) at a ratio of 100:1. Mix well. Incubate in the dark at room temperature for

15 minutes. Add antifade mounting medium and observe using a confocal microscope.

Real-time PCR

Total RNA was extracted from Cultured cells using TRIzol (Thermos) according to the manufacturer's protocol. concentrations of total RNA were measured by NanoDrop 2000 (Thermos). Total RNA was then subjected to gDNA digestion using DNaseI (Byotime), immediately reversed to cDNA followed by EasyScript[®] First-Strand cDNA Synthesis SuperMix (Transgene AE301). Real-Time PCR was performed using FX7 (Thermo Fisher Scientific) and PowerUp[™] SYBR[™] Green Supermix (A25742, Thermo Fisher) following the manufacturer's protocol. The results were analyzed by the thermos express software, and relative expression level was presented as the ratio of the target gene to the endogenous gene, actin. The primer sets for the realtime PCR are listed in Supplementary Table 1.

Live cell imaging to detect nuclear membrane rupture

Mouse nucleophosmin (NP) (NM_001412005.1) fusion with GFP was constructed into pcDNA3.1 and transfected into HEK293 cells using lipo8000TM transfection reagent (beyotime, CO533). Stain the nuclei with NucBlue[™] Live ReadyProbes[™] (Thermo Fisher, R37605) and observe the localization changes in NP-GFP cells.

Mouse nuclear envelope protein Sun1 (NM_024451.2) fusion with GFP was constructed into the pLVX-mCherry vector, packaged into lentivirus, and used to infect HEK293 cells. A stable cell line was selected. Observe the continuous changes of Sun1 fusion with GFP dynamically under a confocal microscope.

Cell immunofluorescence assay

Seed the cells in a confocal dish, treat with drugs or hypoxia for a certain period, and gently wash the slides with PBS 3 times to remove unattached cells. Fix the cells with 4% paraformaldehyde at room temperature for 10-15 minutes. Wash the fixed cells 3 times with PBS. Incubate with 0.1% Triton X-100 at room temperature for 10 minutes. Wash 3 times with PBS. Add 5% BSA and incubate at room temperature for 30 minutes to block non-specific binding. Add the following primary antibodies: TLK2 (1:200, proteintech, 13979-1-AP), non-muscle Myosin IIA (1:200, abcam, ab138498), laminB1 (1:200, abcam, ab16048), γ H2AX (1:200, abcam, ab229914), Nuclear Pore Complex Proteins (1:200, Abcam, ab24609) and incubate overnight. Then incubate with secondary antibodies (goat anti-Mouse IgG/IgM (H + L) (1:1000, Thermo Fisher Scientific, A-10680) and goat anti-Rabbit IgG/IgM (H + L) (1:1000, Thermo Fisher Scientific, A-21428)) at room temperature for 2 hours. Observe cell morphology and staining using a fluorescence microscope or confocal microscope and capture images for analysis.

AAV2 plasmids construction and AAV2 preparation

The pscAAV2/2-GFP plasmid was obtained from Addgene (Plasmid #32396). For AAV2/2 plasmid construction, the pscAAV2/2-GFP coding region was replaced with cre cDNA (coding sequence shown in Supplementary Table 2) and u6 promoter-shRNA (sequence shown in Supplementary Table 2). The AAV2/2 Rap2-Cap2 (Addgene plasmid #104963) and Helper plasmid pAdDeltaF6 (Plasmid #112867) were co-transfected into HEK293T cells. AAV2/2 was purified using PEG8000 precipitation and ultrafiltration methods. The AAV2/2 titer measured by real-time PCR ranged from 1-2 \times 10¹³ genome copies/mL.

Intravitreal injection and optic nerve crush

Adult mice were anesthetized with intraperitoneal injection of tribromoethanol (20 mg/mL). For intravitreal injection, Proparacaine Hydrochloride eye drops were used before surgery. A Hamilton microsyringe (5 μ L) with a 34 G needle was inserted posterior to the ora serrata to inject AAV2/2 or other solutions into the vitreous body. N-

methyl-D-aspartate (MedChemExpress, HY-17551) was prepared in PBS. For optic nerve crush, to fully expose the mouse optic nerve, mice were gently placed under a stereomicroscope following anesthesia, and a drop of proparacaine was applied to each eye to alleviate discomfort. Once deep anesthesia was confirmed, the mouse's head was carefully adjusted to face the operator. Using the tip of a cell forceps, the upper and lower eyelids were gently separated to slightly protrude the eyeball. The conjunctiva at the temporal upper edge of the eyeball was gently pinched with a finger, and a small fold was created using a No. 7 curved forceps. A 1-mm incision was made in the temporal conjunctiva using spring scissors, and the hole was gradually widened with blunt dissection using forceps. The surrounding tissue was gently dissected with cell forceps until the overlying muscle was clearly visible. The cell forceps were passed through the newly created channel, carefully navigating through the muscle and displacing any adipose tissue obstructing the optic nerve. Once the optic nerve was clearly exposed, a jeweler's forceps was inserted approximately 2 mm behind the eyeball, around the optic nerve, and gently released to apply pressure for 10 seconds. The clamp was gently moved back and forth to check if the eyeball moved correspondingly.

Histology and microscopy

For immunohistochemistry, the eyes of mice with attached optic nerves were perfused and surgically removed, fixed with 4% PFA at room temperature for 2 hours. Using a dissecting microscope, the eyes were bisected along the equator, and the cornea, lens, and vitreous were removed. The retina was carefully peeled off intact and any remaining vitreous fibers on the retina were cleaned using fine forceps. The retina was then washed with PBS for 15 minutes, repeated 3 times. The retina was incubated in PBST containing 0.3% Triton X-100 in an EP tube with gentle shaking for 2 hours, followed by fresh PBS washes, repeated 3 times. The retina was blocked with PBS containing 5% BSA (immunofluorescence blocking solution) at room temperature for 2 hours. After washing with PBS 3 times, each for 15 minutes, primary antibodies *tuj1* (1:200, Biolegend, 801202) and RBPMS (1:250, Proteintech, 15187-1-AP) were added in antibody dilution buffer and incubated overnight at 4 °C. The retinas were washed with PBS 3 times, each for 15 minutes, followed by incubation with secondary antibodies goat anti-Mouse IgG/IgM (H + L) (1:1000, Thermo Fisher Scientific, A-10680) and goat anti-Rabbit IgG/IgM (H + L) (1:1000, Thermo Fisher Scientific, A-21428) at room temperature for 2 hours. After washing with PBS 3 times, each for 15 minutes, the retina was mounted on a slide using antifade mounting medium containing DAPI. Data were collected using a Leica SP8 confocal microscope. Sampling and analysis were conducted in square areas around the periphery of each whole-mounted retina (approximately 500 μm from the center to the edge of the retina).

Stimulated emission depletion microscopy (STED)

Super-resolution sample preparation follows the same protocol as conventional immunofluorescence. Cells were seeded onto confocal dishes, fixed with PFA, treated with 0.3% Triton X-100 for 15 minutes, and blocked with 5% BSA for 1 hour. Primary antibodies against Nuclear Pore Complex Proteins (1:100, Abcam, ab24609) and Myosin IIA (1:100, Abcam, ab138498) were added and incubated overnight. Secondary antibodies Goat anti-Rabbit IgG (H + L), Alexa Fluor™ 647 (Thermo Fisher Scientific, A-21244) and Goat anti-Mouse IgG (H + L), Alexa Fluor™ 555 (Thermo Fisher Scientific, A-21424) were added. Images were acquired using the Abberior STEDYCON super-resolution imaging system. Image analysis was performed using ImageJ.

Retrograde tracing of visual pathways

1.5 μl of Cholera Toxin Subunit B (CTB, Alexa Fluor 488 conjugate, Thermo Fisher Scientific, C22841) (2 μg/μl in PBS) was injected into the

vitreous body. Three days post-CTB injection, animals were perfused with 4% PFA. The optic nerves were dissected, fixed, and mounted for imaging.

Visual acuity measurement in visual tasks

This task was performed in a trapezoidal water tank with shallow water. Two screens were placed on either side of the wide end of the tank. One screen displayed a fixed, vertically oriented sine-wave grating, while the other displayed a uniform gray image with the same average luminance. Animals were trained to swim from the narrow end toward the screens and select the screen displaying the grating to escape to a hidden underwater platform beneath it. The training grating had a spatial frequency of 0.054 cycles/degree. During testing, the spatial frequency of the grating was gradually increased in 0.018 cycles/degree increments until the animal made fewer than 7 correct choices out of 10 trials. At least 4 close interruptions were required to determine the animal's visual acuity (spatial frequency threshold). Mice were trained and their visual acuity measured before NMDA-induced injury. From days 1 to 3 post-NMDA injection, mice were tested daily at low (training) spatial frequency to maintain their training activity. From days 4 to 14 post-NMDA injection, the spatial frequency was varied until the threshold was determined for each mouse.

EdU detection of cell proliferation in primary neuron cultures and in mice

For mouse retinal samples, EdU (200 μM) is injected into the mouse eye via intravitreal injection. After 7 days, NMDA treatment is administered at the same injection site. Three days after NMDA treatment, the mice are perfused with 4% PFA, and the retinas are collected. Following fixation, retinas are labeled with RBPMS for routine immunofluorescence staining to identify RGCs. The presence of EdU is then detected using the Click-iT™ reaction (based on Click Chemistry). Alexa Fluor®-488 dye is used in the reaction with EdU to emit fluorescence. Finally, the retinal samples are stained with DAPI to better visualize cell nuclei and EdU-labeled cells under a fluorescence microscope. Fluorescence signals are observed and imaged using a fluorescence or confocal microscope for detection and analysis. For primary mouse neurons, primary cultured neurons are harvested after 4 days, followed by a 48-hour EDU treatment, with or without a 24-hour calcium ionophore treatment. Post 4% PFA fixation, routine immunofluorescence staining is performed, and the Click-iT™ reaction is conducted similarly to the retinal sample procedure.

Statistics and reproducibility

Statistical analyses were conducted using GraphPad Prism software (version 9.5), with data reported as mean ± SD. Between-group comparisons were analyzed using Student's two-tailed t-test with Welch's correction for unequal variances. Multiple group comparisons were evaluated by one-way ANOVA followed by Tukey's post hoc test for homogeneous variance conditions. For multi-variable datasets requiring interaction analysis, two-way ANOVA with Bonferroni correction was applied. Statistical significance thresholds were uniformly defined as: * $P < 0.05$, ** $P < 0.01$, *** $P < 0.001$, **** $P < 0.0001$, with "ns" denoting non-significant outcomes ($P \geq 0.05$). All statistical annotations and methodological specifics are explicitly detailed in corresponding figure legends.

Reporting summary

Further information on research design is available in the Nature Portfolio Reporting Summary linked to this article.

Data availability

All data generated or used in this study are provided in the Supplementary Information. Source data are provided with this paper.

References

1. Kumar, A., Bodhinathan, K. & Foster, T. C. Susceptibility to Calcium Dysregulation during Brain Aging. *Front Aging Neurosci* **1**, 2 (2009).
2. Urbonaviciute, D., Buteikiene, D. & Januleviciene, I. A Review of Neovascular Glaucoma: Etiology, Pathogenesis, Diagnosis, and Treatment. *Medicina* **58**, <https://doi.org/10.3390/medicina58121870> (2022).
3. Arnould, T., Michiels, C., Alexandre, I. & Remacle, J. Effect of hypoxia upon intracellular calcium concentration of human endothelial cells. *J Cell Physiol* **152**, 215–221 (1992).
4. Berna, N., Arnould, T., Remacle, J. & Michiels, C. Hypoxia-induced increase in intracellular calcium concentration in endothelial cells: role of the Na(+)-glucose cotransporter. *J Cell Biochem* **84**, 115–131 (2001).
5. Galluzzi, L. et al. Molecular mechanisms of cell death: recommendations of the Nomenclature Committee on Cell Death 2018. *Cell Death Differ* **25**, 486–541 (2018).
6. Kohda, K., Wang, Y. & Yuzaki, M. Mutation of a glutamate receptor motif reveals its role in gating and delta2 receptor channel properties. *Nat Neurosci* **3**, 315–322 (2000).
7. Syntichaki, P., Xu, K., Driscoll, M. & Tavernarakis, N. Specific aspartyl and calpain proteases are required for neurodegeneration in *C. elegans*. *Nature* **419**, 939–944 (2002).
8. Xu, K., Tavernarakis, N. & Driscoll, M. Necrotic cell death in *C. elegans* requires the function of calreticulin and regulators of Ca(2+) release from the endoplasmic reticulum. *Neuron* **31**, 957–971 (2001).
9. Zhang, Y., Cai, R., Zhou, R., Li, Y. & Liu, L. Tousel-like kinase mediated a new type of cell death pathway in *Drosophila*. *Cell Death Differ* **23**, 146–157 (2016).
10. Verma, M., Wills, Z. & Chu, C. T. Excitatory Dendritic Mitochondrial Calcium Toxicity: Implications for Parkinson's and Other Neurodegenerative Diseases. *Front Neurosci* **12**, 523 (2018).
11. Zhang, Y., Cai, R., Zhou, R., Li, Y. & Liu, L. Tousel-like kinase mediated a new type of cell death pathway in *Drosophila*. *Cell Death & Differentiation* **23**, 146–157 (2016).
12. Liu, C. & Hermann, T. E. Characterization of ionomycin as a calcium ionophore. *Journal of Biological Chemistry* **253**, 5892–5894 (1978).
13. Lee, M.-s et al. Neurotoxicity induces cleavage of p35 to p25 by calpain. *Nature* **405**, 360–364 (2000).
14. Kim, J. A. et al. Comprehensive functional analysis of the tousel-like kinase 2 frequently amplified in aggressive luminal breast cancers. *Nat Commun* **7**, 12991 (2016).
15. Ronald, S. et al. Phenothiazine Inhibitors of TLKs Affect Double-Strand Break Repair and DNA Damage Response Recovery and Potentiate Tumor Killing with Radiomimetic Therapy. *Genes Cancer* **4**, 39–53 (2013).
16. Mortuza, G. B. et al. Molecular basis of Tousel-Like Kinase 2 activation. *Nat Commun* **9**, 2535 (2018).
17. Yagami, T., Yamamoto, Y. & Koma, H. Pathophysiological Roles of Intracellular Proteases in Neuronal Development and Neurological Diseases. *Mol Neurobiol* **56**, 3090–3112 (2019).
18. Mah, L. J., El-Osta, A. & Karagiannis, T. C. gammaH2AX: a sensitive molecular marker of DNA damage and repair. *Leukemia* **24**, 679–686 (2010).
19. Galluzzi, L. et al. Essential versus accessory aspects of cell death: recommendations of the NCCD 2015. *Cell Death Differ* **22**, 58–73 (2015).
20. Kruman, I. I. et al. Cell cycle activation linked to neuronal cell death initiated by DNA damage. *Neuron* **41**, 549–561 (2004).
21. Berridge, M. J. Calcium signalling and cell proliferation. *Bioessays* **17**, 491–500 (1995).
22. Salic, A. & Mitchison, T. J. A chemical method for fast and sensitive detection of DNA synthesis in vivo. *Proc Natl Acad Sci USA* **105**, 2415–2420 (2008).
23. Barbar, E. Dynein light chain LC8 is a dimerization hub essential in diverse protein networks. *Biochemistry* **47**, 503–508 (2008).
24. Vicente-Manzanares, M., Ma, X., Adelstein, R. S. & Horwitz, A. R. Non-muscle myosin II takes centre stage in cell adhesion and migration. *Nat Rev Mol Cell Biol* **10**, 778–790 (2009).
25. Thomas, D. G. et al. Non-muscle myosin IIB is critical for nuclear translocation during 3D invasion. *J Cell Biol* **210**, 583–594 (2015).
26. Limouze, J., Straight, A. F., Mitchison, T. & Sellers, J. R. Specificity of blebbistatin, an inhibitor of myosin II. *J Muscle Res Cell Motil* **25**, 337–341 (2004).
27. McCarty, D. M. Self-complementary AAV vectors; advances and applications. *Mol Ther* **16**, 1648–1656 (2008).
28. Namekata, K. et al. Dock3 attenuates neural cell death due to NMDA neurotoxicity and oxidative stress in a mouse model of normal tension glaucoma. *Cell Death Differ* **20**, 1250–1256 (2013).
29. Lambuk, L. et al. Dose-dependent effects of NMDA on retinal and optic nerve morphology in rats. *Int J Ophthalmol* **12**, 746–753 (2019).
30. Sisk, D. R. & Kuwabara, T. Histologic changes in the inner retina of albino rats following intravitreal injection of monosodium L-glutamate. *Graefes Arch Clin Exp Ophthalmol* **223**, 250–258 (1985).
31. Rodriguez, A. R., de Sevilla Muller, L. P. & Brecha, N. C. The RNA binding protein RBPMS is a selective marker of ganglion cells in the mammalian retina. *J Comp Neurol* **522**, 1411–1443 (2014).
32. Prilloff, S., Noblejas, M. I., Chedhomme, V. & Sabel, B. A. Two faces of calcium activation after optic nerve trauma: life or death of retinal ganglion cells in vivo depends on calcium dynamics. *Eur J Neurosci* **25**, 3339–3346 (2007).
33. Ecker, J. L. et al. Melanopsin-expressing retinal ganglion-cell photoreceptors: cellular diversity and role in pattern vision. *Neuron* **67**, 49–60 (2010).
34. Kumar, A. Calcium Signaling During Brain Aging and Its Influence on the Hippocampal Synaptic Plasticity. *Adv Exp Med Biol* **1131**, 985–1012 (2020).
35. Calvo-Rodriguez, M. et al. Increased mitochondrial calcium levels associated with neuronal death in a mouse model of Alzheimer's disease. *Nat Commun* **11**, 2146 (2020).
36. Bano, D. & Ankarcrona, M. Beyond the critical point: An overview of excitotoxicity, calcium overload and the downstream consequences. *Neurosci Lett* **663**, 79–85 (2018).
37. Neves, D., Salazar, I. L., Almeida, R. D. & Silva, R. M. Molecular mechanisms of ischemia and glutamate excitotoxicity. *Life Sci* **328**, 121814 (2023).
38. Hettiarachchi, N. T. et al. alpha-Synuclein modulation of Ca2+ signaling in human neuroblastoma (SH-SY5Y) cells. *J Neurochem* **111**, 1192–1201 (2009).
39. Betzer, C. et al. Alpha-synuclein aggregates activate calcium pump SERCA leading to calcium dysregulation. *EMBO Rep.* **19**, <https://doi.org/10.15252/embr.201744617> (2018).
40. Hyrc, K., Handran, S. D., Rothman, S. M. & Goldberg, M. P. Ionized intracellular calcium concentration predicts excitotoxic neuronal death: observations with low-affinity fluorescent calcium indicators. *J Neurosci* **17**, 6669–6677 (1997).
41. Mattson, M. P. & Arumugam, T. V. Hallmarks of Brain Aging: Adaptive and Pathological Modification by Metabolic States. *Cell Metab* **27**, 1176–1199 (2018).
42. Wu, D., Sun, J. K. & Chow, K. H. Neuronal cell cycle reentry events in the aging brain are more prevalent in neurodegeneration and lead to cellular senescence. *PLoS Biol* **22**, e3002559 (2024).
43. Herrup, K. & Yang, Y. Cell cycle regulation in the postmitotic neuron: ozymoron or new biology? *Nat Rev Neurosci* **8**, 368–378 (2007).
44. Arendt, T., Bruckner, M. K., Mosch, B. & Losche, A. Selective cell death of hyperploid neurons in Alzheimer's disease. *Am J Pathol* **177**, 15–20 (2010).

45. Chen, M. J. et al. Gene profiling identifies commonalities in neuronal pathways in excitotoxicity: evidence favouring cell cycle re-activation in concert with oxidative stress. *Neurochem Int* **62**, 719–730 (2013).
46. Kodis, E. J., Choi, S., Swanson, E., Ferreira, G. & Bloom, G. S. N-methyl-D-aspartate receptor-mediated calcium influx connects amyloid-beta oligomers to ectopic neuronal cell cycle reentry in Alzheimer's disease. *Alzheimers Dement* **14**, 1302–1312 (2018).
47. Pfaller, R., Smythe, C. & Newport, J. W. Assembly/disassembly of the nuclear envelope membrane: cell cycle-dependent binding of nuclear membrane vesicles to chromatin in vitro. *Cell* **65**, 209–217 (1991).
48. Carrera, P. et al. Tousled-like kinase functions with the chromatin assembly pathway regulating nuclear divisions. *Genes Dev* **17**, 2578–2590 (2003).
49. Taneja, N., Baillargeon, S. M. & Burnette, D. T. Myosin light chain kinase-driven myosin II turnover regulates actin cortex contractility during mitosis. *Mol Biol Cell* **32**, br3 (2021).
50. Perkins, L. A. et al. The Transgenic RNAi Project at Harvard Medical School: Resources and Validation. *Genetics* **201**, 843–852 (2015).

Acknowledgements

This work was supported by the Non-profit Central Research Institute Fund of the Chinese Academy of Medical Sciences (2024-JKCS-11) awarded to LL, as well as by the Beijing Hospitals Authority's Ascent Plan (No. DFL20220505) and the Beijing High-level Public Health Technical Personnel Training Program (Discipline Leader-01-13) awarded to GZ.

Author contributions

Y.L., G.Z., X.C. and L.L. designed the experiments. Y.L., H.H., J.G., J.L., G.K., Y.G. and W.J. performed the experiments. Y.L., H.H., J.G., J.L., G.K., Y.G. and W.J. acquired data. Y.L. and H.H. provided data analysis. Y.L., G.Z. and J.L. wrote the manuscript.

Competing interests

The authors declare no competing interests.

Additional information

Supplementary information The online version contains supplementary material available at <https://doi.org/10.1038/s41467-025-58737-y>.

Correspondence and requests for materials should be addressed to Guojun Zhang or Lei Liu.

Peer review information *Nature Communications* thanks Bingqing Huang, Qun Chen, and the other, anonymous, reviewer(s) for their contribution to the peer review of this work. A peer review file is available."

Reprints and permissions information is available at <http://www.nature.com/reprints>

Publisher's note Springer Nature remains neutral with regard to jurisdictional claims in published maps and institutional affiliations.

Open Access This article is licensed under a Creative Commons Attribution-NonCommercial-NoDerivatives 4.0 International License, which permits any non-commercial use, sharing, distribution and reproduction in any medium or format, as long as you give appropriate credit to the original author(s) and the source, provide a link to the Creative Commons licence, and indicate if you modified the licensed material. You do not have permission under this licence to share adapted material derived from this article or parts of it. The images or other third party material in this article are included in the article's Creative Commons licence, unless indicated otherwise in a credit line to the material. If material is not included in the article's Creative Commons licence and your intended use is not permitted by statutory regulation or exceeds the permitted use, you will need to obtain permission directly from the copyright holder. To view a copy of this licence, visit <http://creativecommons.org/licenses/by-nc-nd/4.0/>.

© The Author(s) 2025